Surface Science 604 (2010) 1813–1819

Contents lists available at ScienceDirect

Surface Science

journal homepage: www.elsevier.com/ locate/susc

Oxygen adsorption on stepped Pd(100) surfaces

F. Li [a], F. Allegretti [a], S. Surnev [a,*], F.P. Netzer [a], Y. Zhang [b,c], W.-B. Zhang [b,c], K. Reuter [b,c]

[a] Institute of Physics, Surface and Interface Physics, Karl-Franzens University Graz, A-8010 Graz, Austria
[b] Fritz-Haber-Institut der Max-Planck-Gesellschaft, Faradayweg 4-6, D-14195 Berlin, Germany
[c] Technische Universität München, Lichtenbergstr. 4, D-85747 Garching, Germany

ARTICLE INFO

Article history:
Received 12 April 2010
Accepted 12 July 2010
Available online 17 July 2010

Keywords:
Synchrotron radiation photoelectron spectroscopy
Density-functional calculations
Chemisorption
Stepped surface
Palladium
Oxygen

ABSTRACT

We use scanning tunneling microscopy (STM) and high-resolution core-level spectroscopy (XPS) measurements to study the initial oxidation of vicinal Pd(100) surfaces exhibiting close-packed (111) steps. The XPS data analysis is supported by detailed surface-core level shift calculations based on density-functional theory. Both STM images and the XPS spectra are found to be perfectly consistent with a characteristic zigzag O decoration of the Pd steps predicted by a preceding cluster-expansion based theoretical study [Y. Zhang and K. Reuter, Chem. Phys. Lett. 465, 303 (2008)]. Continued oxygen uptake leads to the additional stabilization of a $p(2\times2)$-O overlayer on the Pd(100) terraces, and ultimately to step bunching with the resulting large Pd(100) terraces covered by the PdO(101) surface oxide.

1. Introduction

The interaction of oxygen with transition metal surfaces has long gained significant attention in both fundamental and applied research, due to its importance in heterogeneous catalysis and corrosion. For well-defined low-index single crystal surfaces this has established a rather profound understanding, which ranges from the early stages of on-surface oxygen adsorption to the formation of surface- and bulk-oxide phases [1]. Recently and as a step toward higher material's complexity, the interaction of oxygen with vicinal metal surfaces, consisting of periodic arrays of atomic steps, has become an intriguing subject of investigation. Generally anticipated is a significant impact of the modified electronic structure in the vicinity of the lower coordinated step atoms on the surface oxidative and catalytic properties. Seminal studies have indeed already demonstrated that the steps of vicinal transition metal (Pt, Pd, Rh) surfaces exhibit an enhanced reactivity toward oxidation, leading to the formation of novel one-dimensional (1-D) oxidic configurations [2–5].

Understanding their structure at the atomic level is a challenging task, even in the combination of state-of-the-art experimental and theoretical methods. For stand-alone predictive-quality theory the situation is even more daunting, with a most formidable limitation imposed by the vast number of possible geometric configurations. In an attempt to overcome the prevalent approach of simply restricting the calculations to a handful of (chemically motivated) candidate structures, some of us have recently proposed a cluster-expansion based approach for a more systematic exploration of configurational space [6]. In the application to the oxygen adsorption at stepped Pd (100) this identified a large range of oxygen chemical potentials where oxygen atoms decorate alternating sites at close-packed (111) steps in a characteristic Pd–O zigzag structure, with the (100) terraces either empty or covered by a chemisorbed $p(22)$-O layer. At higher chemical potentials more dense oxygen structures form both at the steps and the terraces, signaling the onset of surface oxide formation [6].

While clearly a step forward, the cluster-expansion based structure determination still has its limitations, most notably in that it was restricted to the lattice spanned by on-surface adsorption sites. Its capabilities can therefore not extend to the situation where the formation of oxides is accompanied by substantial substrate rearrangement. The motivation of the present work is therefore to assess the validity of the theoretical predictions with a dual experimental approach that has already proven to be a most powerful tool for unraveling complex surface structures: Atomically resolved imaging of the step structure by scanning tunneling microscopy (STM) combined with core-level photoelectron spectroscopy (XPS) with its intrinsic sensitivity to the local chemical and geometrical environment.

Investigating the adsorption of oxygen on stepped Pd(119) and Pd (1 1 17) surfaces at oxygen pressures below 1×10^{-8} mbar, our STM images fully confirm the predicted zigzag step decoration. Analyzing the complex surface core-level shift (SCLS) data with density-functional theory (DFT) calculations allows even to disentangle

* Corresponding author.
E-mail address: svetlozar.surnev@uni-graz.at (S. Surnev).

0039-6028/$ – see front matter © 2010 Elsevier B.V. All rights reserved.
doi:10.1016/j.susc.2010.07.012

small geometric differences in this zigzag-decoration, depending on whether oxygen is also present at the terraces or not. At higher oxygen pressures the regular step periodicity is not preserved anymore and significant step bunching occurs. While this is outside the realm of the preceding cluster-expansion work, the observed formation of the PdO(101) surface oxide [7,8] on the resulting large Pd(100) terraces concurs again fully with the expectations from previous *ab initio* atomistic thermodynamics studies on this low-index surface [6,9–11].

2. Experimental and computational setup

Two stepped Pd(100) surfaces have been employed in our experimental investigation: Pd(119) and Pd(1 1 17). As illustrated in Fig. 1 both surfaces consist of (100) terraces that are 5 and 9 atom rows wide, respectively, and separated by {111} faceted steps, 12.5 Å and 23.4 Å apart. STM and low-energy electron diffraction (LEED) measurements have been performed in Graz in a custom-designed ultra-high vacuum (UHV) system with a base pressure of 1×10^{-10} mbar, equipped with a variable-temperature AFM-STM (Omicron), four-grid LEED optics and sample heating and cleaning facilities [12]. The STM was operated at room temperature and in a constant current mode. The STM tunneling conditions were set to achieve the best atomic resolution. Depending on the tip termination, bias voltages between a few mV and 1 V have been used. High-resolution XPS experiments have been performed at beamline I311 at MAX-lab, Lund, Sweden [13]. The photoemission spectra have been collected at normal emission angle and photon energies of 120, 400 and 620 eV for the valence band, Pd 3*d* and O 1 *s* core level regions, respectively. The total energy resolution in the present experiments was ~100–200 meV. The vicinal Pd surfaces have been cleaned by 1.5 keV Ar^+–ion sputtering followed by annealing to 1000 K for several minutes, and by heating cycles in O_2 atmosphere at 570 K followed by a final short flash to 1000 K. Oxygen has been introduced into the UHV systems via leak valves at pressures varying between 5×10^{-9} and 5×10^{-7} mbar; the oxygen exposures are given in Langmuir ($1\ \mathrm{L}=1\times10^{-6}$ torr s).

The DFT calculations were performed within the full-potential augmented plane wave (LAPW/APW + lo) framework [14], treating electronic exchange and correlation at the level of the generalized gradient approximation due to Perdew, Burke and Ernzerhof [15]. The Pd(119) surface was described in a supercell setup with symmetric 33 layer slabs, a vacuum separation of 10 Å, (2×1) surface unit-cells, and oxygen adsorption at both sides. All structures were fully relaxed, keeping only the atomic positions in the central two Pd(119) slab layers at their fixed bulk positions. The LAPW/APW + lo basis set parameters are identical to those used in our preceding work on oxygen at vicinal Pd(100) [6,16,17], where also the numerical convergence with respect to the key structural and electronic quantities has already been described in detail. The procedure to obtain initial- and final-state contributions to the SCLSs is exactly the same as detailed in ref. [18], in which the initial-state shifts are simply given by Kohn–Sham eigenvalue differences and the final-state screening is computed within the Slater–Janak transition state approach by an impurity calculation with half an electron removed from the core state considered.

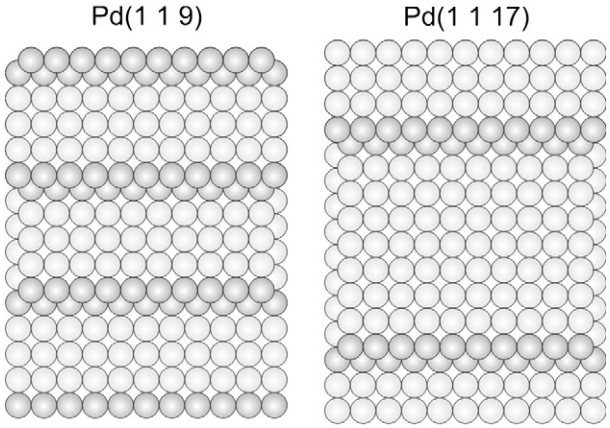

Fig. 1. Schematic top views of the Pd(119) (left) and Pd(1 1 17) (right) surfaces. Step atoms are darkened for clarity.

3. Results and discussion

3.1. Morphology and structure overview

Fig. 2a shows an STM image of the Pd(119) surface exposed to 6 L of oxygen at 5×10^{-9} mbar, with the sample kept at 520 K. To avoid a possible reaction of the chemisorbed oxygen layer with residual gas molecules (such as e.g. CO or H_2) from the UHV background, the sample has been kept at the same oxygen pressure and room temperature during the STM measurements. The STM image reveals a regular array of steps with an average periodicity of 12.5 Å ± 0.2 Å, which is identical with the theoretical step separation of 12.5 Å of the clean Pd(119) surface. The corresponding LEED pattern (inset of

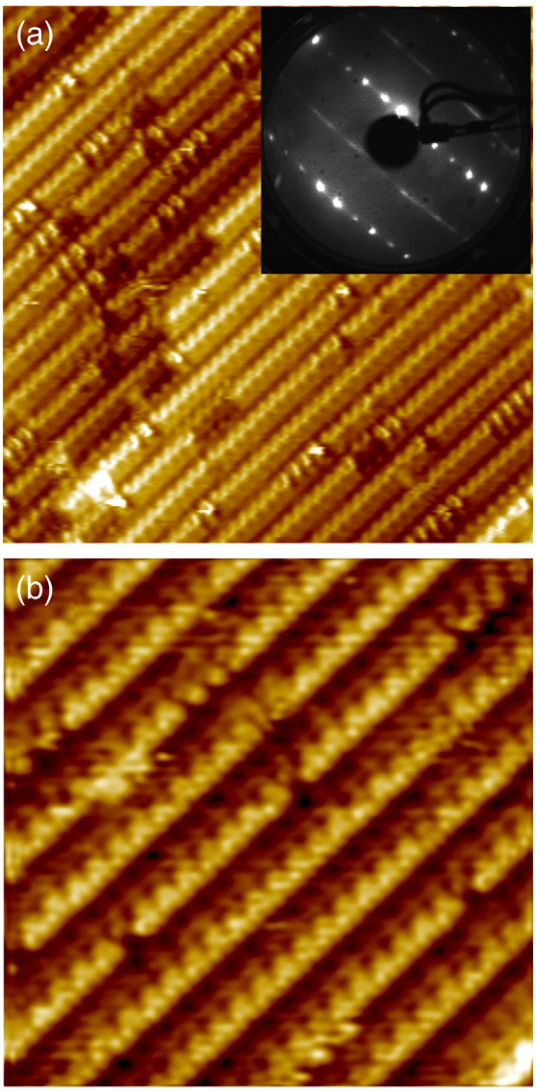

Fig. 2. STM images of the Pd (119) surface after 6 L oxygen dose at 5×10^{-9} mbar and substrate temperature of 520 K: (a) (200Å × 200Å, +1.0 V, 0.1 nA); (b) (100Å × 100Å, +0.4 V, 0.1 nA). The inset in panel a shows the LEED pattern of this surface ($E=65$ eV).

Fig. 2a) shows sharp periodic spot splitting at the integer-order positions, corresponding to the clean Pd(119) surface, confirming that the step periodicity has been preserved after the oxygen adsorption. The streaks at the half-order positions suggest that a well-ordered oxygen superstructure with a (×2) periodicity forms along the step direction, but the structural order across the steps is less perfect. The most prominent feature of the STM image is the zigzag-like appearance of the step edges, which is better recognized in the high-resolution image of Fig. 2b. It shows zigzag chains consisting of two atomic rows separated by 2.9 ± 0.2 Å. Both rows have a periodicity of 5.5 Å along the step direction, which corresponds to twice the Pd(100) lattice constant, in agreement with the observed superstructure periodicity in the LEED pattern. Unfortunately, no information could be gained from the STM images on the structure at the narrow (119) terraces, possibly due to tip shadowing effects near the steps.

For this reason we have investigated the oxygen adsorption also on the Pd(1 1 17) surface, which exhibits wider (100) terraces. The STM image in Fig. 3a shows (100) terraces of uniform width, which are separated by straight step edges at a distance of ~23 Å. This clearly demonstrates that also the step periodicity of the pristine Pd(1 1 17) surface is preserved after a 30 L oxygen dose at 5×10^{-9} mbar oxygen at a sample temperature of 520 K. A square superstructure with a lattice parameter of 5.5 Å can be discerned on the (100) terraces, which is readily attributed to a chemisorbed $p(2 \times 2)$-O layer on a Pd (100) surface [7,19,20]. This is also consistent with the sharp $p(2 \times 2)$ LEED pattern (see inset in Fig. 3a), with the half-order spot exhibiting a splitting perpendicular to the step direction and therewith outlining good structural order of the oxygen adlayer. The high-resolution STM image in Fig. 3b provides further details on the step structure: the 1D zigzag chain (marked with the guiding lines), which we have also observed at the step edges on the Pd(119) surface, can be clearly recognized here. The periodicity along the chain is again 5.5 Å, i.e. twice the Pd lattice constant. The interior zigzag row is spaced by 5.5 Å from the adjacent $p(2 \times 2)$-O terrace row and appears with a brighter (higher) contrast than the edge row. The location of the O adatoms in the $p(2 \times 2)$-O structure is well-known, namely in the fourfold hollow Pd sites [7,11,21]. Tersoff–Hamann style STM simulations furthermore indicate that O appears as bright protrusions at both terrace and step edge. On this basis the STM image allows us to determine the positions of the O atoms adsorbed in the vicinity of the step edges, namely every second fourfold hollow position at the upper Pd step edge in the interior zigzag row. The distance between the two zigzag rows is ≈ 2.8 Å, from which we infer that the exterior edge row corresponds to oxygen adatoms located in the threefold hollow sites at the step (111) facet. This is exactly the structural arrangement that was predicted as most stable configuration for a wide range of O chemical potential in the preceding cluster-expansion based theoretical study [6].

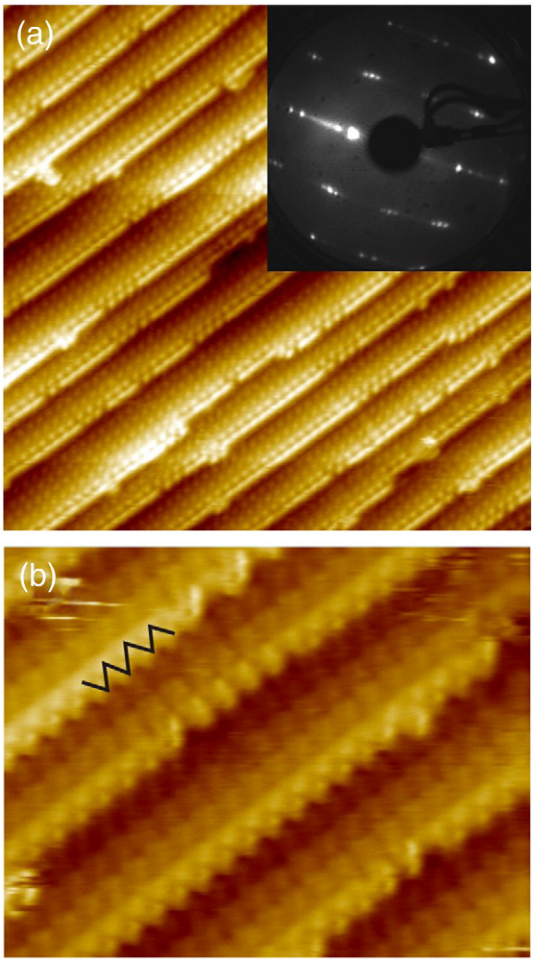

Fig. 3. STM images of the Pd (1 1 17) surface after 30 L oxygen dose at 5×10^{-9} mbar and substrate temperature of 520 K: (a) (250Å × 250Å, +2 mV, 0.1 nA); (b) (100Å × 75Å, +4 mV, 0.1 nA). The inset in Fig. 2a shows the LEED pattern of this surface ($E = 67$ eV).

Exposing the Pd(119) and Pd(1 1 17) surfaces to higher oxygen pressures causes significant step bunching and faceting, as demonstrated in Fig. 4 for the Pd(1 1 17) surface. After an initial oxygen dose of 30 L at 5×10^{-8} mbar and 570 K (Fig. 4a) a large number of kinks develop at the step edges. The (100) terraces still exhibit the $p(2 \times 2)$-O structure, due to the chemisorbed oxygen, but their width is not regular anymore. At an oxygen pressure of 5×10^{-7} mbar step bunching sets in: The STM image in Fig. 4b shows large (100) terraces that are separated by a multitude of monoatomic steps, as visualized on the line profile presented in Fig. 4c. The angle between the (100) terraces and the side facets varies between 9° and 22°, indicating that no preferred facet orientation occurs under the employed oxidation conditions. The high resolution STM image in Fig. 4d has been taken from one of the Pd(100) terraces and demonstrates that the latter are covered by the PdO(101) surface oxide phase, as recognized from its characteristic $(\sqrt{5} \times \sqrt{5})R27°$ periodicity [7,8]. The regular surface step periodicity can be restored after shortly flashing the facetted surface in UHV to 1000 K.

3.2. Core-level and valence band spectra

To get more insight into the initial oxygen build-up on the stepped Pd(100) surfaces we have investigated the evolution of core-level and valence band photoemission spectra with the oxygen dose. In these experiments the Pd(119) surface (with the larger step density) has been employed in order to enhance the effect of the step structure on the core-level line shapes. We also concentrate on the Pd $3d_{3/2}$ spectrum, as it exhibits a higher surface sensitivity due to a more favorable photoelectron kinetic energy compared to the Pd $3d_{5/2}$ one. In order to avoid the step bunching and surface faceting described in the previous section, the oxygen pressure was kept at the lower value of 5×10^{-9} mbar. The Pd substrate has been kept at 90 K during the oxygen exposure and flashed afterwards briefly to 300 K to induce ordering in the oxygen adlayer (exposing the Pd(119) surface directly at 300 K to oxygen yields similar results).

Fig. 5 shows the measured evolution of the Pd $3d_{3/2}$ (a), O 1 *s* (b) core-level and valence band (c,d) photoemission spectra as a function of the oxygen dose on the Pd(119) surface. Dosing of up to 0.2 L oxygen obviously causes a quenching of low binding energy SCLS components in the Pd $3d_{3/2}$ line shape at the expense of some transfer of spectral weight to the high binding energy side of the peak. On further oxygen exposure the Pd $3d_{3/2}$ peak shape becomes symmetrically broadened and eventually after a saturation dose of about 5 L

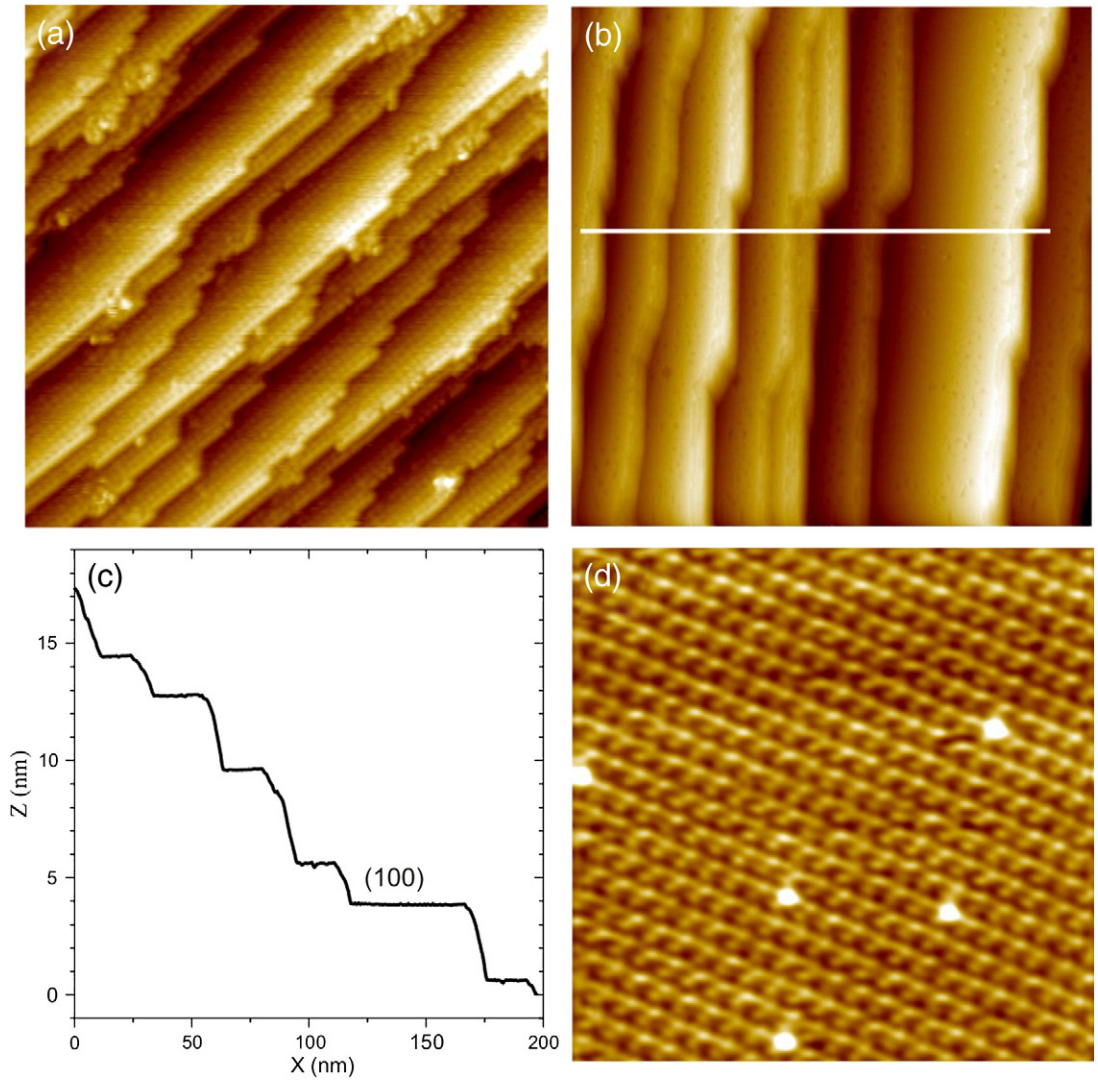

Fig. 4. STM images of the Pd (1 1 17) surface (a) after a 30 L oxygen dose at 5×10^{-8} mbar (300Å × 300Å, +1.5 V, 0.1 nA) and (b) after a 100 L dose at 5×10^{-7} mbar (2000Å × 2000Å, +1.5 V, 0.1 nA). The sample temperature during the oxidation was 570 K. (c) Line profile along the line indicated in panel b. (d) STM images of the flat terrace in panel b, displaying the $(\sqrt{5}\times\sqrt{5})R27°$ structure of the PdO surface oxide.

an additional shoulder develops at the high binding energy side. The corresponding O1*s* spectra (Fig. 5b) are unfortunately significantly obscured by the overlapping dominant Pd $3p_{3/2}$ peak. To eliminate the contribution of the latter we have determined its shape parameters for the clean Pd(119) surface and kept it fixed to fit the combined O 1 *s* – Pd 3*p* spectra. The peak-fit analysis yields a single O 1 *s* component (blue curves in Fig. 5b) with a binding energy which varies only insignificantly between 529.25 eV at low oxygen dose and 529.15 eV at saturation. The integrated O 1 *s* intensity has been plotted versus the oxygen dose (uptake curve) in Fig. 5e and confirms that saturation is reached after a dose of 2 L. This O uptake and saturation are also nicely seen in the valence band spectra (Fig. 5c, d), where the increase in spectral intensity at about 5 eV and close to the Fermi-level reflects the formation of bonding and anti-bonding states at the lower and upper edge of the Pd band as predicted by Newns–Anderson theory [1].

From the observed saturation and our STM results we expect that the final Pd $3d_{3/2}$ spectrum taken after 5 L oxygen dose corresponds to the situation where the $p(2\times2)$-O + zigzag step phase is fully developed. In the following we therefore subject this spectrum and the one from the clean surface to a peak deconvolution analysis and compare to computed SCLSs for the corresponding structures. The recorded spectrum of the clean Pd(119) surface is shown in the left panel of Fig. 6. The corresponding calculated final-state SCLSs with respect to the Pd bulk atoms of the different Pd (119) surface atoms, following the labeling provided in the right panel of Fig. 6, are given in Table 1 and schematically summarized in the form of bars below the spectrum. Determining essentially zero SCLSs for all 2nd layer atoms, the calculations predict three major components: One component from the three middle terrace atoms Pd2–Pd4 shifted by -330 ± 10 meV from the bulk peak, as well as one component each from the Pd atoms at the upper (Pd1) and lower (Pd5) step edge with negative SCLSs of −425 meV and −198 meV, respectively. The decomposition of the experimental spectrum into four corresponding components (bulk plus three times surface) also shown in Fig. 6 yields indeed a perfect match after only marginal (within ±100 meV) reoptimization of the binding energies and peak heights. The full width at half maximum (FWHM) and asymmetry of the individual core level components have been determined to be 0.75 ± 0.05 eV and 0.15 ± 0.05, respectively.

In the left panel of Fig. 7 we perform a corresponding analysis of the Pd $3d_{3/2}$ spectrum taken after a saturation oxygen dose of 5 L. The calculated final-state SCLSs for the $p(2\times2)$-O + zigzag step model shown in the right panel of Fig. 7 are again summarized below the spectrum, with the explicit values given in Table 2. They reveal an

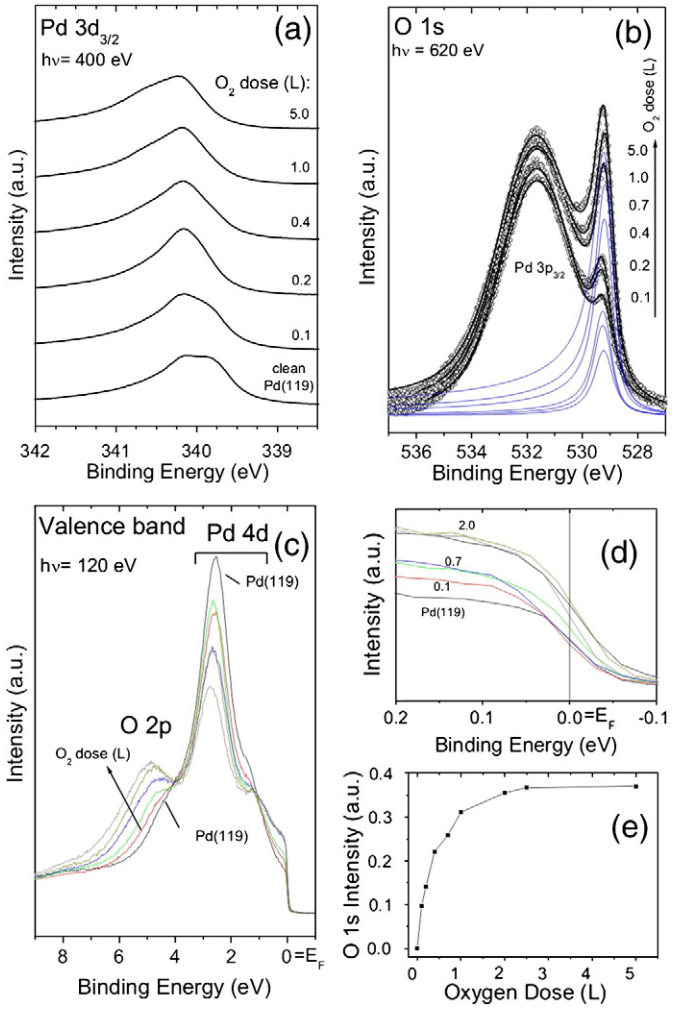

Fig. 5. Evolution of the core level Pd $3d_{3/2}$ (a), O *1 s* (b) and valence band spectra (c) as a function of the oxygen dose on the Pd(119) surface. Panel d is an enlargement of panel c near the Fermi level. The O *1 s* spectra have been fitted together with the Pd $3p_{3/2}$ line shapes (see text) and the resulting oxygen uptake is plotted in panel e.

Table 1
Computed initial-state, screening correction and final-state SCLSs for the clean Pd(119) surface. The labels for the different atoms follow the notation given in Fig. 6. All values are given in meV.

Atom	Δ initial SCLS	Δ screen SCLS	Δ final SCLS
Pd1	−535	110	−425
Pd2	−462	123	−339
Pd3	−453	129	−324
Pd4	−454	116	−339
Pd5	−238	40	−198

intriguing complexity beyond what one would expect from simply accounting for the number of directly coordinated O atoms. In such a view, the similarly coordinated upper step atoms Pd1 and Pd2 should exhibit roughly similar SCLSs, while the actually computed values differ by about 150 meV, cf. Table 2. The same holds for the difference of atoms Pd3 and Pd4, and in turn their largely different SCLSs compared to those of the other terrace atoms Pd5–Pd8. The reason for this symmetry breaking is that the position of the upper step edge O atom, denoted Thu in Fig. 7, does not really correspond to the ideal fourfold hollow site. Instead it is better described as a quasi-threefold coordination, with the Thu O atom much stronger bound to the Pd4 atom with a bond length of 2.01 Å than to the Pd3 atom with a bond length of 2.83 Å. As a result, the computed SCLSs divide roughly into four groups that comprise in parts seemingly inequivalent Pd surface atoms, cf. Fig. 7: One component at -400 ± 20 meV due to the essentially zerofold O-coordinated atoms Pd3 and Pd10, one centered around the bulk peak from the terrace atoms Pd5–Pd8, one component at 330 ± 40 meV due to Pd4 and Pd9, and finally an even further shifted component due to the most strongly O-coordinated Pd1 and Pd2 atoms at the upper step edge. As shown in Fig. 7 a corresponding deconvolution of the experimental spectrum into four components yields indeed an excellent fit after only minor optimization of the binding energies to A (−370 meV), B (0 meV), C (+330 meV) and D (+580 meV). We also note that despite the different coordination, the computed O1*s* binding energies of the three O adatoms Thp, Thu and Sh2, cf. Fig. 7, differ by less than 250 meV, which is fully consistent with the single component resolved in the experimental spectrum shown in Fig. 5b.

The threefold-hollow-like adsorption geometry of O atoms at the Thu and Sh2 step sites is further confirmed by high-resolution

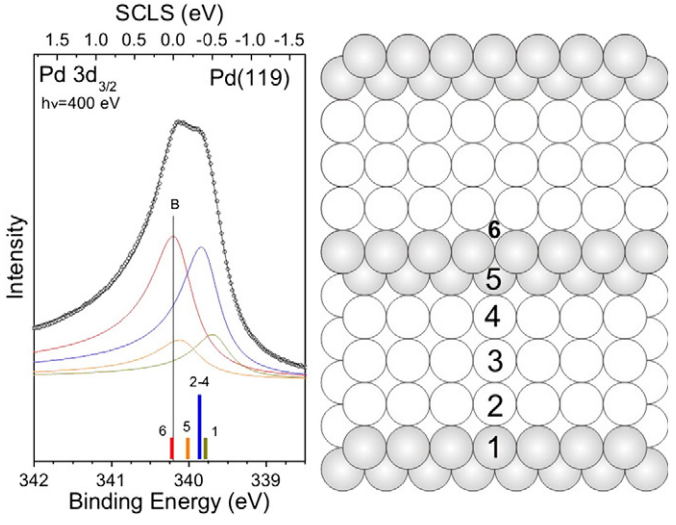

Fig. 6. (left panel) Peak decomposition analysis of the Pd $3d_{3/2}$ line shape of the clean Pd (119) surface. The calculated SCLSs for the clean surface are displayed as bars at the bottom (see Table 1), following the notation for the different Pd surface atoms given in the schematic top view in the right panel.

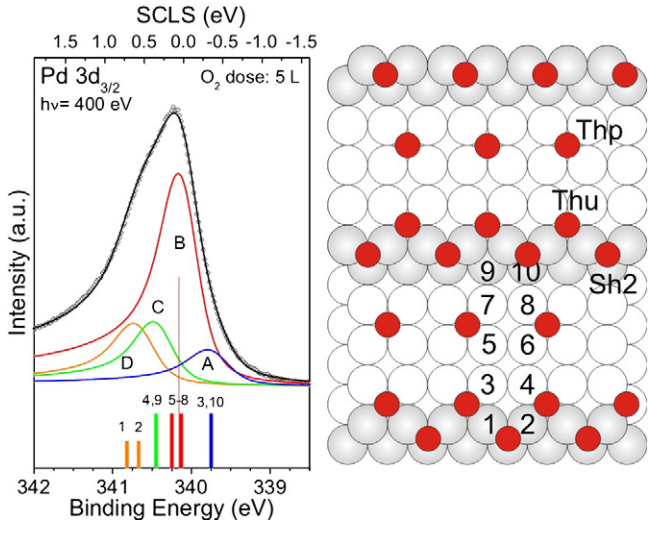

Fig. 7. (left panel) Peak decomposition analysis of the Pd $3d_{3/2}$ line shape of the Pd(119) surface exposed to 5 L O_2 at 5×10^{-9} mbar. The calculated SCLSs for the $p(2\times2)$-O + zigzag step model are displayed as bars at the bottom (see Table 2), following the notation for the different Pd surface atoms given in the schematic top view in the right panel.

Table 2
Computed initial-state, screening correction and final-state SCLSs for the $p(2\times2)$-O + zigzag step model of the Pd(119) surface. The labels for the different atoms follow the notation given in Fig. 7. All values are given in meV.

Atom	Δ initial SCLS	Δ screen SCLS	Δ final SCLS
Pd1	428	276	704
Pd2	296	255	551
Pd3	−534	123	−410
Pd4	193	100	293
Pd5	−108	83	−25
Pd6	8	85	94
Pd7	−8	92	84
Pd8	−113	76	−37
Pd9	295	73	368
Pd10	−490	107	−383

electron energy loss spectroscopy (HREELS) data of the p(2x2)-O + zigzag step decorated Pd(1 1 17) surface [22]. The HREELS spectrum contains a major loss peak at 44 meV, which is due to vibrations of atomic oxygen in fourfold hollow (Thp) sites on the Pd (100) terraces [23]. In addition, a shoulder at about 55 meV is resolved, which is associated with oxygen atoms decorating the Pd steps. The latter loss is characteristic of threefold coordinated chemisorbed O species, as on a Pd(111) surface [24].

The overall shift of spectral intensity toward higher binding energies at increasing O exposure is perfectly consistent with the general expectation for an increasing O load at the surface. Furthermore, the preceding paragraph has shown that the measured O-induced peak shape at saturation can be fully rationalized by the $p(2\times2)$-O + zigzag step model. Closer inspection of the evolution of the Pd $3d_{3/2}$ spectrum with oxygen dose shown in Fig. 5a nevertheless reveals that already at the lowest O_2 dose of 0.1 L there are significant changes away from the spectrum of the clean surface, but also still different from the one at saturation. An immediate explanation would be that oxygen only decorates the more reactive step edge at this low dosage, but does not yet form the $p(2\times2)$-O superstructure at the terrace. As mentioned initially, a corresponding structure with O exclusively forming the zigzag pattern at the step edge has indeed also been predicted by the cluster-expansion based theoretical study for a narrow range of chemical potentials [6]. Stabilization of such an initial structure would obviously rationalize the still higher spectral weight at lower binding energies. On the other hand, if oxygen decorates the step in the same zigzag fashion as at saturation, the highest binding energy components due to the Pd step atoms should be very similar. However, the shoulder at highest binding energies clearly develops only at the saturation dosage in Fig. 5a. This can be further quantified by subjecting the spectrum at 0.1 L dose to the same four component deconvolution as done for the case at saturation before. Fig. 8 demonstrates that this yields in fact an excellent fit to the data, with those components containing contributions from the terrace atoms located at the lower binding energies as expected. Not withstanding, also the highest energy component D is now located 80 meV lower than at saturation. The solution to this puzzle comes from the actually calculated SCLSs for the zigzag step model shown in the right panel of Fig. 8. Without the terrace O atoms present, the upper step edge Thu O adatom now exhibits an almost ideal fourfold coordination with bond lengths to its four Pd neighbors all in the range 2.14–2.16 Å. As apparent from Table 3, the strong symmetry breaking of the SCLSs induced by the quasi threefold Thu adsorption site in the $p(2\times2)$-O + zigzag step structure is thus absent. This implies, in particular, that also the most strongly O-coordinated Pd1 atom that exhibits a SCLS of +704 meV in the saturation structure now shows a much lower SCLS of +533 meV. As demonstrated in Fig. 8, this together with the other computed SCLSs therewith achieves a similarly good rationalization of the experimental line shape as at the saturation coverage discussed before.

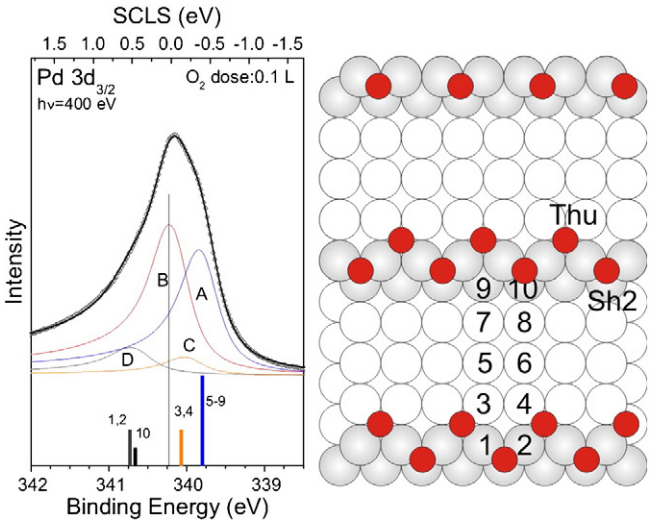

Fig. 8. (left panel) Peak decomposition analysis of the Pd $3d_{3/2}$ line shape of the Pd(119) surface exposed to 0.1 L O_2 at 5×10^{-9} mbar. The calculated SCLSs for the zigzag step model are displayed as bars at the bottom (see Table 3), following the notation for the different Pd surface atoms given in the schematic top view in the right panel.

4. Summary and conclusions

In conclusion we have presented detailed STM and high-resolution XPS data to address the initial oxidation of vicinal Pd surfaces exhibiting (100) terraces and close-packed (111) steps. Supported by a detailed SCLS analysis through DFT calculations our measurements indicate a rapid oxygen decoration of the (111) steps in a characteristic (2×1) zigzag pattern, followed by the formation of a $p(2\times2)$-O overlayer on the terraces. Further oxygen uptake leads to step bunching and faceting, with the resulting large (100) terraces covered with the PdO(101) surface oxide.

The determined Pd–O zigzag step structure agrees perfectly with the one predicted previously by a first-principles cluster-expansion based theory study [6]. In this structure O atoms occupy alternating fourfold and threefold hollow sites offered at the upper and lower step edge, respectively. An intriguing detail revealed by the SCLSs analysis is that the formation of the $p(2\times2)$-O overlayer at the terraces at increasing exposure changes the coordination of the upper step edge O atoms from fourfold to quasi-threefold. This is an interesting feature as oxygen is also threefold coordinated to Pd atoms in the PdO(101) surface oxide. The DFT determined geometry shows furthermore that the switch to quasi-threefold coordination is accompanied by a significant outward displacement of the Pd atoms at the step edge row, in fact by close to 100% of the corresponding interlayer distance in the clean surface. This suggests to view the thereby somewhat detached O–Pd–O zigzag trilayer chain along the step edge rather as a 1D precursor toward the surface oxide rather than as a mere O adatom decoration of the Pd step.

Table 3
Computed initial-state, screening correction and final-state SCLSs for the zigzag step model of the Pd(119) surface. The labels for the different atoms follow the notation given in Fig. 8. All values are given in meV.

Atom	Δ initial SCLS	Δ screen SCLS	Δ final SCLS
Pd1	345	188	533
Pd2	343	189	532
Pd3	−191	62	−129
Pd4	−198	63	−135
Pd5	−443	123	−319
Pd6	−425	130	−295
Pd7	−473	129	−344
Pd8	−432	129	−303
Pd9	−427	106	−322
Pd10	397	66	463

References

[1] K. Reuter, Nanometer and sub-nanometer thin oxide films at surfaces of late transition metals, in: U. Heiz, U. Landman (Eds.), Nanocatalysis, Springer, Berlin, ISBN: 978-3-540-32645-8, 2006, pp. 343–376.
[2] J.G. Wang, W.X. Li, M. Borg, J. Gustafson, A. Mikkelsen, T.M. Pedersen, E. Lundgren, J. Weissenrieder, J. Klikovits, M. Schmid, B. Hammer, J.N. Andersen, Phys. Rev. Lett. 95 (2005) 256102.
[3] J. Gustafson, A. Resta, A. Mikkelsen, R. Westerström, J.N. Andersen, E. Lundgren, J. Weissenrieder, M. Schmid, P. Varga, N. Kasper, X. Torrelles, S. Ferrer, F. Mittendorfer, G. Kresse, Phys. Rev. B: 74 (2006) 035401.
[4] R. Westerström, J. Gustafson, A. Resta, A. Mikkelsen, J.N. Andersen, E. Lundgren, N. Seriani, F. Mittendorfer, M. Schmid, J. Klikovits, P. Varga, M.D. Ackermann, J.W.M. Frenken, N. Kasper, A. Stierle, Phys. Rev. B: 76 (2007) 155410.
[5] J. Klikovits, M. Schmid, L.R. Merte, P. Varga, R. Westerström, A. Resta, J. Gustafson, J.N. Andersen, A. Mikkelsen, F. Mittendorfer, G. Kresse, Phys. Rev. Lett. 101 (2008) 266104.
[6] Y. Zhang, K. Reuter, Chem. Phys. Lett. 465 (2008) 303.
[7] M. Todorova, E. Lundgren, V. Blum, A. Mikkelsen, S. Gray, J. Gustafson, M. Borg, J. Rogal, K. Reuter, J.N. Andersen, M. Scheffler, Surf. Sci. 541 (2003) 101.
[8] P. Kostelník, N. Seriani, G. Kresse, A. Mikkelsen, E. Lundgren, V. Blum, T. Šikola, P. Varga, M. Schmid, Surf. Sci. 601 (2007) 1574.
[9] K. Reuter, M. Scheffler, Appl. Phys. A 78 (2004) 793.
[10] J. Rogal, K. Reuter, M. Scheffler, Phys. Rev. Lett. 98 (2007) 046101.
[11] J. Rogal, K. Reuter, M. Scheffler, Phys. Rev. B: 75 (2007) 205433.
[12] F. Allegretti, C. Franchini, V. Bayer, M. Leitner, G. Parteder, B. Xu, A. Fleming, M.G. Ramsey, R. Podloucky, S. Surnev, F.P. Netzer, Phys. Rev. B: 75 (2007) 224120.
[13] R. Nyholm, J.N. Andersen, U. Johansson, B.N. Jensen, I. Lindau, Nucl. Instrum. Methods Phys. Res., Sect. A 467 (2001) 520.
[14] Techn. Universität Wien, Austria3-9501031-1-2, 2001.
[15] J.P. Perdew, K. Burke, M. Ernzerhof, Phys. Rev. Lett. 77 (1996) 3865.
[16] Y. Zhang, J. Rogal, K. Reuter, Phys. Rev. B: 74 (2006) 125414.
[17] Y. Zhang, V. Blum, K. Reuter, Phys. Rev. B 75 (2007) 235406.
[18] S. Lizzit, A. Baraldi, A. Groso, K. Reuter, M.V. Pirovano-Ganduglia, C. Stampfl, M. Scheffler, M. Stichler, C. Keller, W. Wurth, D. Menzel, Phys. Rev. B 63 (2001) 205419.
[19] T.W. Orent, S.D. Bader, Surf. Sci. 115 (1982) 323.
[20] G.W. Simmons, Y.-N. Wang, J. Markos, K. Klier, J. Phys. Chem. 85 (1991) 4522.
[21] K.H. Rieder, W. Stocker, Surf. Sci. 150 (1985) L66.
[22] F. Allegretti, private communication.
[23] G.W. Simmons, Y.-N. Wang, J. Marcos, K. Klier, J. Phys. Chem. 95 (1991) 4522.
[24] F. Leisenberger, G. Koller, M. Sock, S. Surnev, M.G. Ramsey, F.P. Netzer, B. Klötzer, K. Hayek, Surf. Sci. 445 (2000) 380.